Computational Model for Cyclic Mobility and Associated Shear Deformation

Zhaohui Yang, A.M.ASCE[1]; Ahmed Elgamal, M.ASCE[2]; and Ender Parra[3]

Abstract: In saturated clean medium-to-dense cohesionless soils, liquefaction-induced shear deformation is observed to accumulate in a cycle-by-cycle pattern (cyclic mobility). Much of the shear strain accumulation occurs rapidly during the transition from contraction to dilation (near the phase transformation surface) at a nearly constant low shear stress and effective confining pressure. Such a stress state is difficult to employ as a basis for predicting the associated magnitude of accumulated permanent shear strain. In this study, a more convenient approach is adopted in which the domain of large shear strain is directly defined by strain space parameters. The observed cyclic shear deformation is accounted for by enlargement and/or translation of this domain in deviatoric strain space. In this paper, the model formulation details involved are presented and discussed. A calibration phase is also described based on data from laboratory sample tests and dynamic centrifuge experiments (for Nevada sand at a relative density of about 40%).

DOI: 10.1061/(ASCE)1090-0241(2003)129:12(1119)

CE Database subject headings: Liquefaction; Constitutive models; Cyclic plasticity; Soil dynamics; Centrifuge models.

Introduction

In saturated clean medium-to-dense sands (relative densities D_r of about 40% or above, Lambe and Whitman 1969), the mechanism of liquefaction-induced cyclic mobility may be illustrated by the undrained stress-controlled simple shear response of Fig. 1 (Arulmoli et al. 1992). Fig. 1 shows the following:

1. Cycle-by-cycle degradation in shear stiffness manifested by the occurrence of increasingly larger shear strain excursions;
2. A major portion of the large cyclic shear deformation rapidly developing at nearly constant, low shear stress and effective confinement; and
3. A regain of shear stiffness and strength following these large shear strain excursions, along with an increase in effective confinement (due to dilatancy).

The response mechanism in Fig. 1 is representative of a large number of undrained laboratory tests on Nevada sand with D_r of about 40% and above (Arulmoli et al. 1992). Early pioneering studies (Seed and Lee 1966; Castro 1969; Casagrande 1975; Seed 1979) described this pattern of response as a mechanism of cyclic mobility or cyclic liquefaction (National Research Council 1985).

For the important situations of lateral spreading or biased strain accumulation due to the superimposition of static shear stress (e.g., embankment slopes, below foundations, behind retaining walls, etc.), cyclic mobility may play a dominant role (see, e.g., Dobry et al. 1995; Dobry and Abdoun 1998; Balakrishnan and Kutter 1999). The results of an undrained triaxial test with static shear stress bias (Fig. 2) (Arulmoli et al. 1992) show a net increment of permanent strain accumulates in a preferred ''downslope'' direction on a cycle-by-cycle basis. Modeling the magnitude of such increments is of utmost importance in determining the total accumulated permanent deformation (Iai 1998; Dafalias and Manzari 1999; Li et al. 2000).

A number of constitutive models have been developed to simulate cyclic mobility and/or flow-liquefaction soil response (Prevost 1985; Lacy 1986; Pastor and Zienkiewicz 1986; Wang et al. 1990; Iai 1991; Proubet 1991; Bardet et al. 1993; Jefferies 1993; Anandarajah 1993; Aubry et al. 1993; Muraleetharan et al. 1994; Byrne and McIntyre 1994; Tateishi et al. 1995; Borja et al. 1999; Papadimitriou et al. 2001; Arduino et al. 2001). Among the notable recent advances is the successful implementation of the state-dependent-dilatancy concept (Manzari and Dafalias 1997; Cubrinovski and Ishihara 1998a,b; Li and Dafalias 2000). This concept is implemented by explicit incorporation of the void ratio into the constitutive model, which allows the various soil response characteristics (contraction/dilation, cyclic-mobility/flow liquefaction) to be elegantly reproduced within a unified plasticity framework.

Currently, reliable computational modeling of the accumulated shear deformation associated with cyclic mobility still remains a major challenge. As indicated above, a major portion of these deformations develops at a state of low nearly constant shear stress and effective confinement (Figs. 1 and 2). This minimal change in stress state at very low confinement levels poses a significant challenge to reliably reproducing the associated shear deformation (using traditional stress–space models). Therefore, an effort is made in this study to model such deformations directly by a strain–space yield domain, within classical multisurface (stress–space) plasticity formulation (Parra 1996; Yang 2000). The observed cyclic shear deformation patterns are then accounted for by enlargement and/or translation of this domain in strain space.

It is of interest to note that stress– and strain–space formula-

[1]Research Fellow, Dept. of Structural Engineering, Univ. of California, San Diego, La Jolla, CA 92093.

[2]Professor, Dept. of Structural Engineering, Univ. of California, San Diego, La Jolla, CA 92093.

[3]Integrated Production Manager, PDVSA, INTEVEP, Urbanización Santa Rosa, Los Teques, P.O. Box 76343A, Caracas 1070A, Venezuela.

Note. Discussion open until May 1, 2004. Separate discussions must be submitted for individual papers. To extend the closing date by one month, a written request must be filed with the ASCE Managing Editor. The manuscript for this paper was submitted for review and possible publication on June 22, 2000; approved on February 24, 2003. This paper is part of the ***Journal of Geotechnical and Geoenvironmental Engineering***, Vol. 129, No. 12, December 1, 2003. ©ASCE, ISSN 1090-0241/2003/12-1119–1127/$18.00.

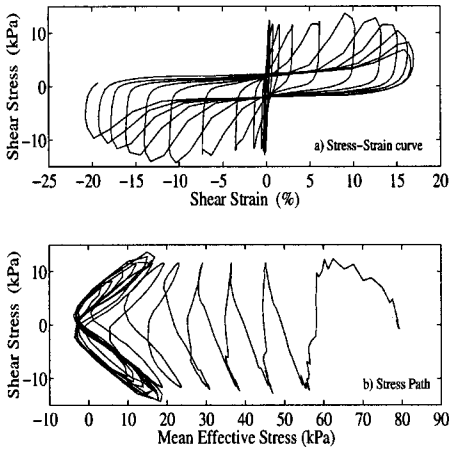

Fig. 1. Stress–strain and stress–path response for Nevada sand ($\mathbf{D}_r = 60\%$) in a stress-controlled, undrained cyclic simple shear test (Arulmoli et al. 1992)

tions have been combined in earlier studies. For instance, in a model developed for concrete materials, Bazant and Kim (1979) used a stress–space loading function for plastic deformation and a strain–space counterpart for fracturing (strain-softening) deformation. In our case, since the micromechanics governing accumulation of cyclic shear deformation (Figs. 1 and 2) remain a topic of research, the strain–space mechanism introduced is a phenomenological approach that allows reproducing the experimentally observed response.

The constitutive model developed was incorporated into a solid–fluid fully coupled finite element (FE) code (Chan 1988; Parra 1996). Model calibration was carried out for Nevada sand at about 40% D_r, based on (i) a series of monotonic and cyclic laboratory tests (Arulmoli et al. 1992) and (ii) level-ground and infinite-slope centrifuge model simulations (Taboada 1995; Dobry et al. 1995). In the following, the formulation of this computational framework and the calibration process are presented and discussed.

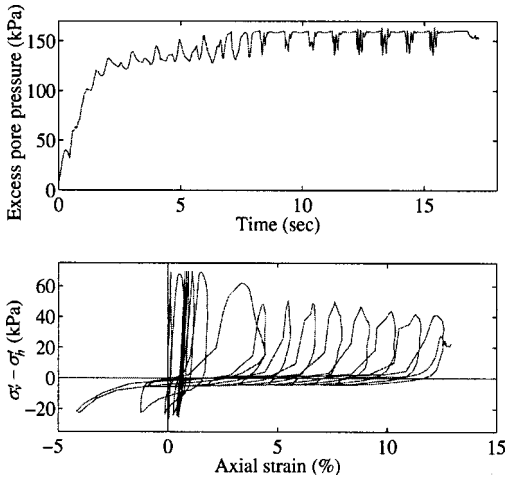

Fig. 2. Excess-pore-pressure and stress–strain histories in an undrained, anisotropically consolidated stress-controlled cyclic triaxial test of Nevada sand at $\mathbf{D}_r = 40\%$ [stress bias 21.5 kPa (Arulmoli et al. 1992)]

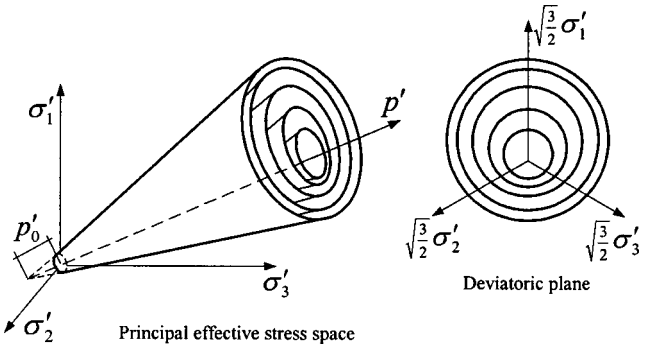

Fig. 3. Conical yield surfaces in principal stress space and deviatoric plane (after Prevost 1985, Parra 1996, and Yang 2000)

Constitutive Model

The main effort reported here is concerned with details of the mechanisms introduced for simulating cyclic plastic shear–strain accumulation. First, we present the necessary components of the classical stress–space formulation based on the original multisurface-plasticity framework of Prevost (1985). Thereafter, discussions are focused on a new nonassociative flow rule and the strain–space mechanism (Parra 1996; Yang 2000), the key elements in reproducing the salient cyclic mobility features in Figs. 1 and 2. Here, the sign convention adopted is such that volumetric stresses/strains are positive in compression.

Yield Function

Following standard convention, it is assumed that material elasticity is linear and isotropic, and that nonlinearity and anisotropy result from plasticity (Hill 1950). The yield function (Fig. 3) is selected as a conical surface in principal stress space (Prevost 1985; Lacy 1986):

$$f = \tfrac{3}{2}[\mathbf{s} - (p' + p_0')\boldsymbol{\alpha}]:[\mathbf{s} - (p' + p_0')\boldsymbol{\alpha}] - M^2(p' + p_0')^2 = 0 \tag{1}$$

in the domain $p' \geqslant 0$, where $\mathbf{s} = \boldsymbol{\sigma}' - p'\boldsymbol{\delta}$ is the deviatoric stress tensor ($\boldsymbol{\sigma}'$ = effective Cauchy stress tensor; $\boldsymbol{\delta}$ = second-order identity tensor); p' = mean effective stress; p_0' = a small positive constant (1.0 kPa in this paper) such that the yield surface size remains finite at $p' = 0$ (for numerical convenience and to avoid ambiguity in defining the yield surface normal at the yield surface apex); α = a second-order deviatoric tensor that defines the yield surface center in deviatoric stress subspace, M defines the yield surface size; and ":" denotes a doubly contracted tensor product. In the context of multisurface plasticity (Iwan 1967; Mroz 1967; Prevost 1985), the hardening zone is defined by a number of similar yield surfaces (Fig. 3) with a common apex (at $-p_0'$ along the hydrostatic axis). The outermost surface is designated as the failure surface, the size of which (M_f) is related to the friction angle ϕ by $M_f = 6\sin\phi/(3 - \sin\phi)$ (Chen and Mizuno 1990).

As described by Prevost (1985), the yield surfaces may be initially configured with nonzero $\boldsymbol{\alpha}$ to account for shear strength difference between triaxial compression and extension. However, it is realized that the Lode angle effect is not incorporated into the current model since the yield function [Eq. (1)] does not include the third stress invariant. Load paths that depend significantly on this effect will not be reproduced satisfactorily. Effort is currently being directed toward inclusion of the third stress invariant in the yield function.

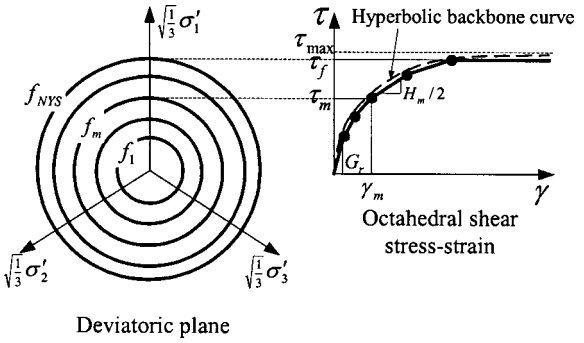

Fig. 4. Hyperbolic backbone curve for soil nonlinear shear stress–strain response and piecewise-linear representation in multisurface plasticity (after Prevost 1985 and Parra 1996)

Shear Stress–Strain Response

In geotechnical engineering practice, nonlinear shear behavior is commonly described by a shear stress–strain backbone curve (Kramer 1996). The backbone curve at a given reference confinement p'_r can be approximated by the hyperbolic formula (Kondner 1963; Duncan and Chang 1970; see Fig. 4):

$$\tau = G_r\gamma/(1+\gamma/\gamma_r) \tag{2}$$

where τ and γ=octahedral shear stress and strain, respectively; G_r=low-strain shear modulus at p'_r (Fig. 4); and $\gamma_r = \tau_{\max}/G_r$, in which $\tau_{\max}$ is the maximum shear strength when γ approaches ∞. In order to reach the maximum shear strength at finite strain, the hyperbolic curve is often capped at $\tau_f < \tau_{\max}$ (Fig. 4). During the calibration process (see "Model Calibration"), τ_f was selected to correspond to shear strain γ of 10% at $p'_r = 80$ kPa.

Within the framework of multisurface plasticity, the hyperbolic backbone curve [Eq. (2)] is replaced by a piecewise linear approximation (Fig. 4). Each linear segment (Fig. 4) represents the domain of a yield surface f_m, characterized by elastoplastic (tangent) shear modulus H_m and size M_m, for $m = 1,2,\ldots,$NYS, where NYS is the total number of yield surfaces (Prevost 1985). At the reference confinement p'_r, H_m is conveniently defined by (see Fig. 4):

$$H_m = 2(\tau_{m+1}-\tau_m)/(\gamma_{m+1}-\gamma_m) \tag{3}$$

with $H_{\text{NYS}} = 0$. Using Eq. (1), the size of surface f_m is now dictated by (see Fig. 4):

$$M_m = 3\tau_m/\sqrt{2}(p'_r + p'_0) \tag{4}$$

with $M_{\text{NYS}} = M_f$ and $\tau_{\text{NYS}} = \tau_f$.

Finally, low-strain shear modulus G is assumed to vary with confinement p' as follows (Prevost 1985):

$$G = G_r[(p'+p'_0)/(p'_r+p'_0)]^n \tag{5}$$

where n=material parameter (=0.5 typically for sand; Kramer 1996). The tangent shear moduli [Eq. (3)] were assumed to follow the same confinement dependence rule [Eq. (5)]. Based on elasticity theory, the bulk modulus of the soil skeleton, B, is defined by $B = 2G(1+\nu)/(3-6\nu)$, where ν is the Poisson ratio.

Hardening Rule

Following Mroz (1967) and Prevost (1985), a purely deviatoric kinematic hardening rule was employed to generate hysteretic response. In our numerical implementation experience, the original surface-translation hardening rule (Mroz 1967) was found to demand a high level of computational effort (particularly at low confinement levels where yield surfaces are of increasingly small size in the deviatoric plane; Fig. 3). In such cases, even with relatively small stress increments, the updated stress state may still fall outside the trajectory of surface translation, and the consistency condition could not be satisfied. Use of smaller load increments to remedy this problem was found to be prohibitively expensive (e.g., in boundary value problem FE computations), and sometimes practically impossible. Thus, in order to enhance computational efficiency, a new yield surface translation rule was developed (Parra 1996). This new logic maintains the Mroz (1967) concept of conjugate-point contact.

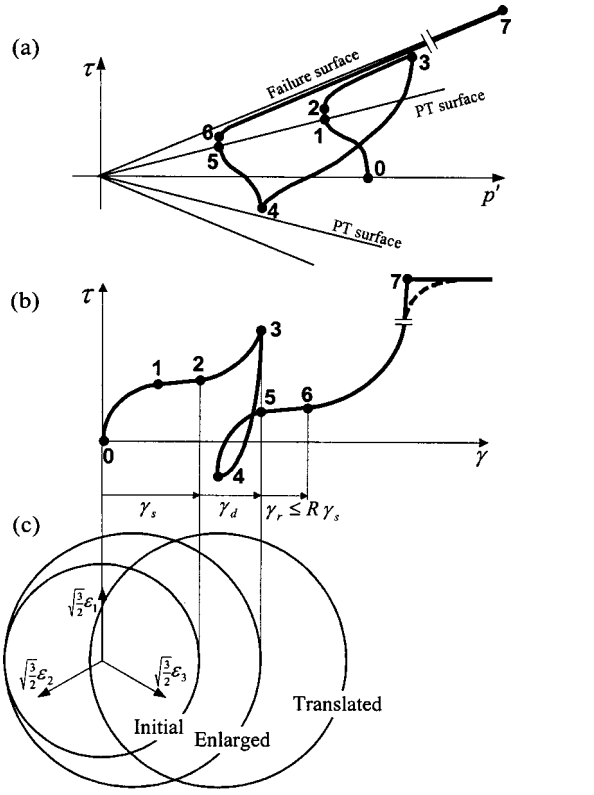

Fig. 5. Schematic of constitutive model response showing (a) octahedral stress τ, effective confinement p' response, (b) octahedral stress τ, octahedral strain γ response, and (c) configuration of yield domain

Flow Rule

We define **Q** and **P** as the outer normal to the yield surface and the plastic potential surface, respectively. These tensors may be conveniently decomposed into deviatoric and volumetric components, giving $\mathbf{Q} = \mathbf{Q}' + Q''\boldsymbol{\delta}$ and $\mathbf{P} = \mathbf{P}' + P''\boldsymbol{\delta}$ (Prevost 1985). Nonassociativity of the plastic flow is restricted to its volumetric component (Prevost 1985), i.e., $\mathbf{Q}' = \mathbf{P}'$ and $P'' \neq Q''$.

Liquefaction studies (Ishihara et al. 1975) have established the concept of the phase transformation (PT) surface (Fig. 5). Under undrained conditions, shear loading inside (or outside) the PT surface is accompanied by a tendency of volume contraction (or dilation), resulting in increased (or decreased) pore pressure and decreased (or increased) p' (Fig. 5). The relative location of the stress state with respect to the PT surface may be inferred (Pre-

vost 1985) from the stress ratio $\eta \equiv \sqrt{3(\mathbf{s}:\mathbf{s})/2}/(p'+p'_0)$. Designating η_{PT} as the stress ratio along the PT surface, it follows that $\eta < \eta_{PT}$ (or $\eta > \eta_{PT}$) if the stress state is inside (or outside) the PT surface.

In our model, depending on the value of η and the sign of $\dot{\eta}$ (the time rate of η), distinct contractive/dilative (dilatancy) behavior is reproduced by specifying appropriate expressions for P''. In addition, a neutral phase ($P''=0$, phase 1–2 in Fig. 5) is proposed between the contraction ($P''>0$, phase 0–1) and the dilation ($P''<0$, phase 2–3) phases. This neutral phase conveniently allows one to model the accumulation of highly yielded shear strain, as will be discussed below.

Contractive Phase (Phases 0–1, 3–4, and 4–5 in Fig. 5)

Shear-induced contraction occurs inside the PT surface ($\eta < \eta_{PT}$), as well as outside ($\eta > \eta_{PT}$) when $\dot{\eta} < 0$. Based on experimental observations (e.g., by Ishihara et al. 1975; Ladd et al. 1977) and micromechanical explanations (Nemat-Nasser and Tobita 1982; Papadimitriou et al. 2001), the rate of contraction is dictated to a significant extent by preceding dilation phase(s). Dafalias and Manzari (1999) addressed this important aspect in their bounding-surface sand model by incorporating a second-order fabric tensor in the dilatancy parameter (equivalent to P'' here) as a function of the plastic volumetric strain ε_v^p accumulated during dilation. Alternatively, Papadimitriou et al. (2001) defined the plastic modulus as a scalar function of ε_v^p. Following their approaches, a simple version is adopted here by specifying P'' as a scalar function of ε_v^p. In particular, the contraction flow rule is defined by

$$P'' = [1 - \text{sign}(\dot{\eta})\eta/\eta_{PT}](c_1 + c_2\varepsilon_c) \tag{6}$$

where c_1 and c_2=positive calibration constants that dictate the rate of contraction (or excess pore pressure increase); and ε_c is a non-negative scalar governed by the following rate equation:

$$\dot{\varepsilon}_c = \begin{cases} -\dot{\varepsilon}_v^p & (\varepsilon_c > 0 \text{ or } -\dot{\varepsilon}_v^p > 0) \\ 0 & (\text{otherwise}) \end{cases} \tag{7}$$

where $\dot{\varepsilon}_v^p$=rate of plastic volumetric strain. In other words, ε_c increases only during dilation and decreases during subsequent unloading (contraction), until it reaches zero (in phase 0–1 in Fig. 5, since no prior dilation has taken place; ε_c remains zero). Thus, a stronger dilation phase (e.g., phase 2–3) results in a higher rate of contraction upon unloading (phase 3–4).

Dilative Phase (Phases 2–3 and 6–7 in Fig. 5)

Dilation appears only due to shear loading outside the PT surface ($\eta > \eta_{PT}$ with $\dot{\eta} > 0$), and is defined here by

$$P'' = (1 - \eta/\eta_{PT}) d_1 (\gamma_d)^{d_2} \tag{8}$$

where d_1 and d_2=positive calibration constants; and γ_d=octahedral shear strain accumulated during this dilation phase. Eq. (8) dictates a dilation tendency that increases with accumulated strain γ_d, as experimentally observed by Kabilamany and Ishihara (1990), and incorporated into the sand model of Cubrinovski and Ishihara (1998a) using an alternative expression.

Critical-State Response (beyond Stage 7 in Fig. 5)

Continued dilation (phase 6–7) may result in significant increases in shear stress and effective confinement. Eventually, the critical state (Casagrande 1936, 1975; Castro 1969) may be attained, whereupon further shear deformation continues to develop without additional volume or confinement changes. As mentioned earlier, this response mechanism [represented by the dashed line segment near stage 7 in Fig. 5(b)] was naturally incorporated into state (void ratio) dependent soil models (of, e.g., Jefferies 1993; Manzari and Dafalias 1997; Cubrinovski and Ishihara 1998a; Li and Dafalias 2000).

Currently, our model lacks a formal expression for state dependence. However, simple logic has been incorporated to remedy this discrepancy, such that volume remains constant ($P''=0$) when the critical state is reached [stage 7, Fig. 5(b)]. Following earlier implementations (Jefferies 1993; Manzari and Dafalias 1997; Li and Dafalias 2000), the critical state is defined based on a relationship between volumetric strain ε_v and effective confinement p'. This response phase is not further pursued here, since it was not observed in the available laboratory and centrifuge experiments employed for model calibration.

Table 1. Model Parameters Calibrated for Undrained $D_r = 40\%$ Nevada Sand

Main calibration experiment	Parameter	Value
CIDC tests	Shear modulus, G_r	33.3 MPa
	Friction angle, ϕ	31.4°
RPI centrifuge model 1	Contraction parameter, c_1	0.075
RPI centrifuge model 2	Phase transformation angle, ϕ_{PT}	26.5°
	Dilation parameter, d_1	200.0
	Dilation parameter, d_2	1.5
	Contraction parameter, c_2	1,000.0
CAUCyclic test	p_y	10.0 kPa
	$\gamma_{s_{max}}$	1.5%
	R	1.0

Neutral Phase (Phases 1–2 and 5–6 in Fig. 5)

As the shear stress increases (Fig. 5, phase 0–1), the stress state eventually reaches the PT surface ($\eta = \eta_{PT}$). At sufficiently high p' levels, dilation (phase 2–3) would follow. However, when p' is low (e.g., 10 kPa or lower in the calibration phase below; see Table 1), a significant amount of permanent shear strain may accumulate prior to dilation (Figs. 1 and 2), with minimal changes in shear stress and p' (implying $P'' \approx 0$).

Such a minimal change in the stress state is difficult to employ as a basis for modeling the associated extent of shear strain accumulation (during which $P'' \approx 0$). Hence, for simplicity, $P''=0$ is maintained during this high yielding phase (phase 1–2), until a boundary defined in deviatoric strain space is reached [Fig. 5(c)], with subsequent dilation thereafter (phase 2–3). This boundary defines an initially isotropic domain in deviatoric strain space [Fig. 5(c)] as a circle of radius γ_s (expressed in terms of octahedral shear strain). This domain will enlarge or translate depending on load history, as described below.

Configuration of Yield Domain. The shear strain γ_d accumulated during dilation [phase 2–3, Fig. 5(b)] may enlarge the yield domain [Fig. 5(c)]. Specifically, enlargement occurs when shear strain accumulated in the current dilation phase exceeds the maximum γ_d the material has ever experienced before (since phase 2–3 is the first time the material experiences dilation, the domain enlarges throughout). This logic preserves the symmetric pattern of cyclic shear deformation observed in Fig. 1, and may be physically interpreted as a form of a damage effect.

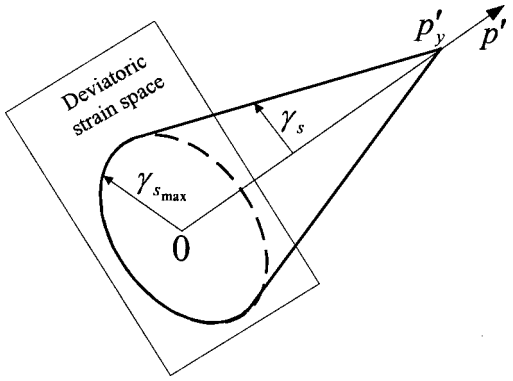

Fig. 6. Initial yield domain at low levels of effective confinement

The presence of superimposed static shear stress results in biased accumulation of shear deformations, discussed earlier (Fig. 2). This biased accumulation is achieved through translation of the yield domain in deviatoric strain space (strain-induced anisotropy; Bazant and Kim 1979), allowing yield increment γ_r to develop before subsequent dilation (phase 5–6, Fig. 5). According to experimentally documented accumulation patterns (Arulmoli et al. 1992; Ibsen 1994), strain increment γ_r is proportional to the level of previous unloading strain (phase 3–4), limited to a maximum of $R\gamma_s$ where R is a user-defined constant. Note that translation of the yield domain continues until the strain accumulated during dilation reaches the maximum γ_d recorded previously [e.g., phase 2–3 in Fig. 5(b)]. Thereafter, the domain enlarges again (the damage effect described above).

The initial yield domain size γ_s depends on effective confinement p'. In the current model, this dependence is defined by the following simple linear relationship (see Fig. 6):

$$\gamma_s = \gamma_{s_{max}} \left\langle \frac{p'_y - p'}{p'_y} \right\rangle \tag{9}$$

where p'_y (10 kPa, Table 1) and $\gamma_{s_{max}}$ (1.5% octahedral strain, Table 1)=model constants that may be easily derived from data such as that shown in Fig. 7. In Fig. 7, the model response under undrained monotonic loading conditions at various low confinement levels clearly indicates the influence of confinement on the extent of accumulated shear strain. Other forms of confinement dependence may easily be prescribed, as dictated by available experimental data.

In Fig. 7, model response under drained monotonic shear loading is also depicted for low confinements (from 1.0 to 10 kPa). However, it should be emphasized that drained volumetric response at very low confinement levels (Sture et al. 1998) is not addressed by the current formulation.

Model performance under symmetric cyclic shear loading is depicted in Fig. 8(a). Fig. 8 shows the combined effect of gradual confinement decrease and dilation history (γ_d) on shear stress–strain response. Fig. 8(b) shows that under biased cyclic loading, the extent of cycle-by-cycle deformation is conveniently simulated via the parameter R.

In summary, the model framework was developed to reproduce the observed salient characteristics associated with liquefaction-induced shear deformation. The incorporated modeling mechanisms may be further refined as more reliable data sets become available. For instance, physically based formulations may eventually replace the neutral phase, and the setting of $P''=0$ within the neutral phase and upon reaching the critical state.

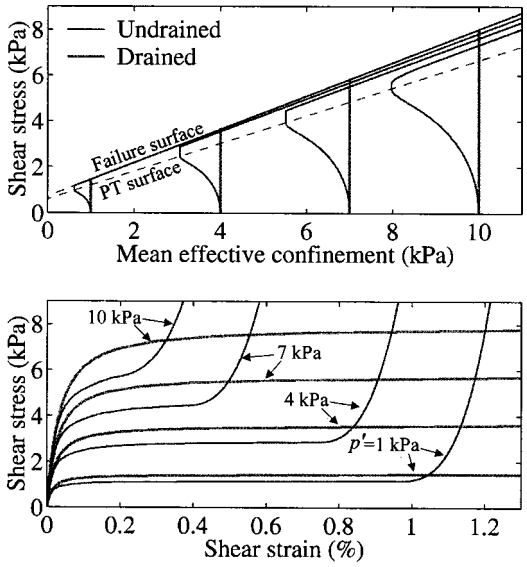

Fig. 7. Undrained and drained monotonic simple shear stress–path and stress–strain responses showing dependence of initial yield domain size on effective confinement

Model Calibration

Calibration was carried out for Nevada sand at about 40% D_r. This calibration phase included the following:

1. Configuration of yield surfaces (defining H_m and M_m) based on data from a set of monotonic consolidated isotropically drained compression (CIDC) tests;
2. Evaluation of the strain–space parameters based mainly on the matching recorded response in a consolidated anisotropically undrained cyclic (CAUCyclic) test; and
3. Evaluation of the shear-volume coupling (dilatancy) parameters through simulations of two dynamic centrifuge tests

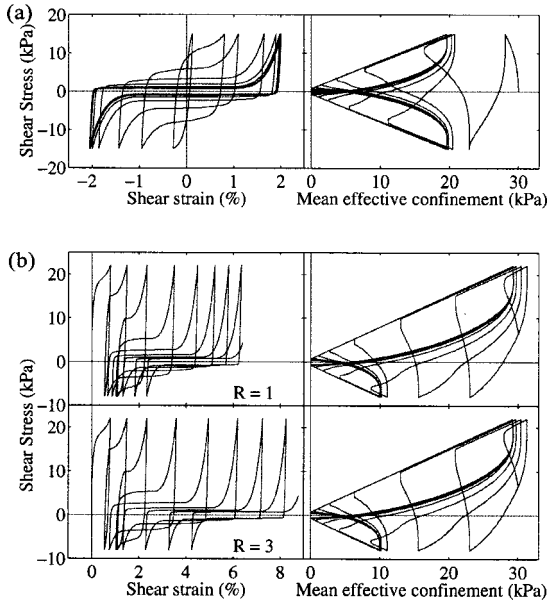

Fig. 8. (a) Model simulation of undrained cyclic simple shear response (stress-controlled simulation at ±15 kPa) and (b) effect of parameter R on undrained cyclic shear response (stress-controlled simulations at ±15 kPa with 7 kPa static shear–stress bias)

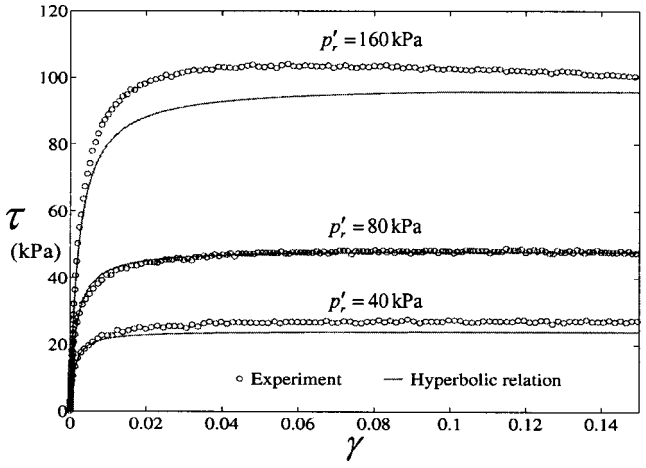

Fig. 9. Backbone curves for Nevada sand at $\mathbf{D}_r = 40\%$ based on isotropically consolidated drained triaxial tests (Arulmoli et al. 1992) and hyperbolic representation

(dealing with liquefied site response and lateral spreading). These centrifuge experiment simulations were conducted using a solid–fluid fully coupled FE program (Parra 1996) that incorporated the constitutive model developed.

The calibration effort attempted to obtain a satisfactory overall match of the entire data set employed, with emphasis on liquefaction-induced shear–strain accumulation mechanisms. In the following, each experimental phase employed is briefly described, along with recorded responses and calibration results. All calibrated modeling parameters are listed in Table 1.

Drained Monotonic Triaxial Test

The monotonic CIDC test was conducted using Nevada sand at about 42% initial D_r (Arulmoli et al. 1992). In this test, the sample was first isotropically consolidated into an effective confining pressure p'_r of 80 kPa. Thereafter, the vertical pressure was gradually increased, with the lateral confining pressure simultaneously decreased, so that p'_r remained constant throughout the test. Thus, the (octahedral) shear stress–strain response recorded during this test generated a backbone curve at 80 kPa confining pressure (Fig. 9).

In order to identify G_r and γ_r, a least-squares curve fitting procedure was performed (Yang 2000) to match the hyperbolic relation [Eq. (2)] to the backbone curve (Fig. 9). Thereafter, yield-surface parameters H_m and M_m were calculated using Eqs. (3) and (4) for each surface f_m (18 surfaces were used, i.e., NYS $=18$). It should be noted that the properties identified also resulted in a reasonable match to two additional CIDC experiments conducted at $p'_r = 40$ and 160 kPa (Arulmoli et al. 1992).

Undrained Cyclic Triaxial Test

An undrained cyclic triaxial test was conducted on Nevada sand at about 39% D_r (Arulmoli et al. 1992). The soil sample was first consolidated to mean effective confinement of 160 kPa, with a 20 kPa difference between the vertical (σ'_1) and the lateral ($\sigma'_2 = \sigma'_3$) principal stresses (anisotropic consolidation or stress bias). Thereafter, the sample was undrained, and stress-controlled harmonic load was applied vertically at frequency of about 1 Hz.

The test was numerically simulated (Fig. 10) using the constitutive model. In this test, the level of deformation was consistent

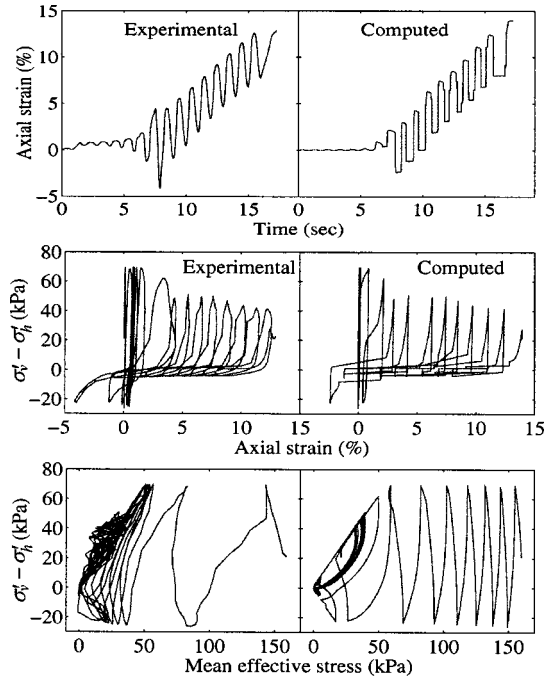

Fig. 10. Recorded and computed results of anisotropically consolidated, undrained cyclic triaxial test (Nevada sand at $\mathbf{D}_r = 40\%$) with static stress bias (Arulmoli et al. 1992)

with the centrifuge model 2 experiment discussed below. Therefore, the parameters controlling cycle-by-cycle accumulation of shear strain were calibrated by matching the last nine cycles of this triaxial test (Fig. 10).

It may be noted that a sudden large pore pressure buildup occurred during the first two loading cycles of this experiment (Fig. 10). However, a second essentially identical triaxial test (test No. 40–50, Arulmoli et al. 1992) did not display similar behavior (i.e., pore-pressure buildup was not consistent between these two experiments, making this part of the data unreliable). Thus, pore pressure development was based on the centrifuge data discussed below, which suggested the gradual buildup mechanism in the numerical response in Fig. 10.

Centrifuge Experiments

Dobry and Taboada (1994) proposed and conducted a number of centrifuge model tests to simulate one-dimensional (1-D) dynamic response of level and mildly sloping sand sites [Fig. 11(a)]. These tests (Taboada 1995) were performed in a 1-D laminated container. Nevada sand was used at a D_r in the range of 40–45%. The centrifuge models attempted to simulate a prototype soil layer of 10 m depth and infinite lateral extent, with a permeability coefficient of 3.3×10^{-3} m/s (Taboada 1995; Dobry et al. 1995).

The results of two models were employed for model calibration/verification, including [see Fig. 11(a)]:

1. VELACS model 1, representing a level site, subjected mainly to 2 Hz harmonic base excitation; and
2. VELACS model 2, representing a mildly inclined infinite slope with an effective inclination angle of about 4°, subjected mainly to 2 Hz harmonic base excitation.

The two tests were simulated using a fully coupled FE program that incorporated the constitutive model (Parra 1996; Yang 2000). Fig. 11(b) shows the finite element mesh, in which a 9–4-

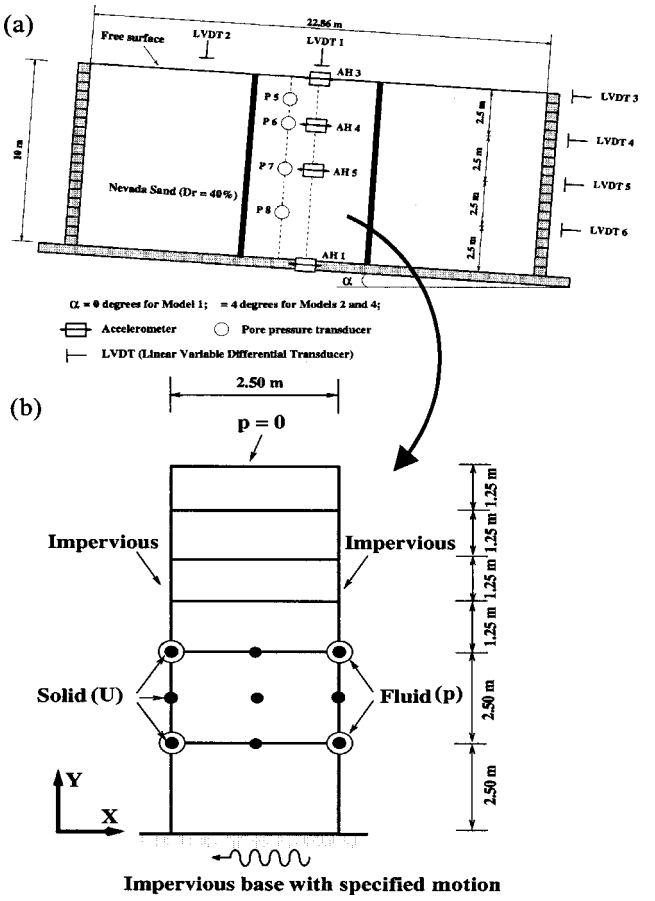

Fig. 11. Centrifuge configurations of RPI models 1 and 2 (Dobry et al. 1995), finite element discretization, and boundary conditions for numerical simulations

node element (9 nodes for the solid phase, and 4 nodes for the fluid phase) was employed (Yang 2000).

In the level-ground case of model 1, the relatively low (symmetric) shear strain during shaking (Fig. 12) led to soil response predominantly below the PT line (i.e., the virtual absence of a dilative tendency). Therefore, this model was employed mainly to calibrate the pore-pressure buildup parameter c_1 [Fig. 13(a)].

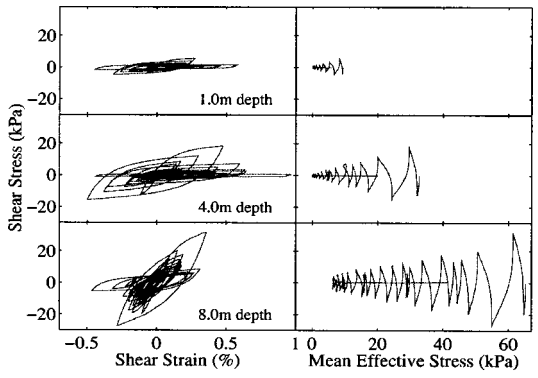

Fig. 12. Computed shear stress strain and stress path at different depths for VELACS model 1 (level ground)

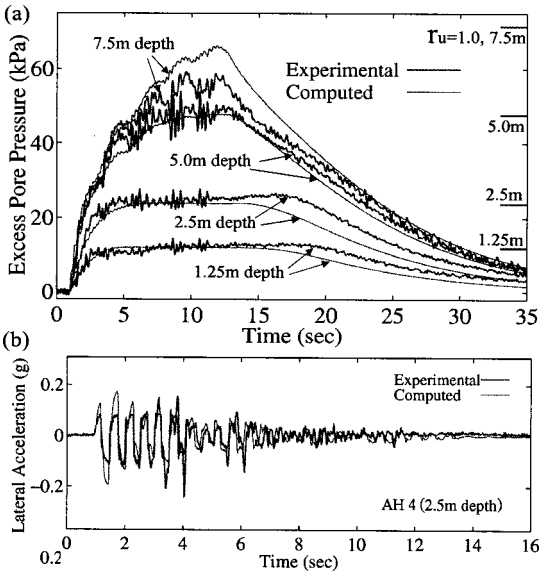

Fig. 13. Computed and experimental excess pore pressure and acceleration time histories for VELACS model 1 (level ground)

Minimal permanent displacements occurred in this case, and a good match was noted between computed and recorded accelerations [Fig. 13(b)].

In model 2, the presence of static driving shear stress due to gravity (4° inclination) led to shear–strain accumulation and strong dilative response in the down-slope direction (Fig. 14). The results of this model were used to calibrate the dilation parameters (η_{PT}, d_1, and d_2), as well as parameter c_2. As shown in Fig. 15, the calibrated parameters (Table 1) resulted in a reasonable match between the recorded and computed lateral displacements at different depths and accelerations (shown at 2.5 m depth).

Remark: The numerically predicted settlement due to liquefaction was generally smaller than observations. Models 1 and 2 resulted in settlement in the range of 0.1–0.2 m, which was considerably underpredicted (numerical estimates were less than 0.05 m). Such large volume changes and their relatively rapid rate of accumulation (entirely during the shaking phase) are currently the topic of further investigation.

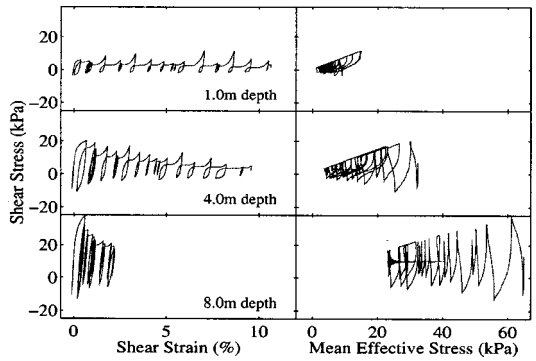

Fig. 14. Computed shear stress strain and stress path at different depths for VELACS model 2 (4° inclination)

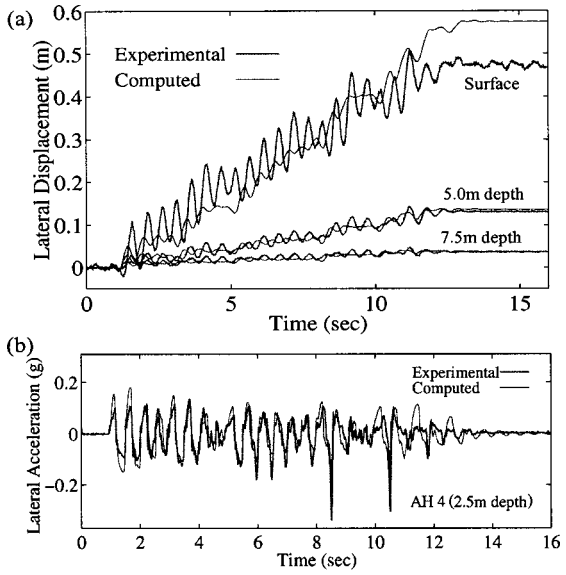

Fig. 15. Computed and experimental lateral displacement and acceleration time histories for VELACS model 2 (4° inclination)

Summary and Conclusions

A constitutive model was developed for numerical simulation of cyclic liquefaction response and associated accumulation of cyclic shear deformation observed in clean sand and silt. Accuracy in predicting such deformation is of the utmost practical significance in structural/foundation stability and damage assessments. Within a stress–space plasticity framework, the model employs a new flow rule and strain–space parameters to simulate the cyclic development and evolution of plastic shear strain. Here, the presentation focused on the development and performance of these key elements. A calibration phase for medium Nevada sand was described, based on a set of laboratory sample experiments and centrifuge liquefaction tests. Overall, the model reproduced the salient cyclic-mobility response characteristics consistently displayed in this experimental data set reasonably well.

Acknowledgments

This work was supported by the Pacific Earthquake Engineering Research (PEER) Center under National Science Foundation Award No. EEC-9701568. The authors are grateful to Dr. Kandiah Arulmoli (Earth Mechanics Inc., Irvine, Calif.), Professor Ricardo Dobry (Rensselaer Polytechnic Inst.), and Professor Victor Taboada (Universidad Nacional Autonoma de Mexico) for providing the experimental data sets. Professor Yannis Dafalias (U. C. Davis) and Professor Majid Manzari (George Washington Univ.) kindly provided valuable suggestions and insights, and their advice is most appreciated.

References

Anandarajah, A. (1993). ''VELACS project: Elasto-plastic finite element predictions of the liquefaction behavior of centrifuge model Nos. 1, 3 and 4a.'' *Proc., Int. Conf. on the Verification of Numerical Procedures for the Analysis of Soil Liquefaction Problems*, K. Arulanandan and R. F. Scott, eds., Balkema, Rotterdam, The Netherlands, 1, 1075–1104.

Arduino, P., Kramer, S., and Baska, D. (2001). ''UW-sand: A simple constitutive model for liquefiable soils.'' *2001 Mechanics and Materials Summer Conf.*, ASME Materials and Applied Mechanics Div., ASCE Engineering Mechanics Div., and Soc. of Engineering Science.

Arulmoli, K., Muraleetharan, K. K., Hossain, M. M., and Fruth, L. S. (1992). ''VELACS: Verification of liquefaction analyses by centrifuge studies, laboratory testing program, soil data report.'' *Project No. 90-0562*, The Earth Technology Corporation, Irvine, Calif.

Aubry, D., Benzenati, I., and Modaressi, A. (1993). ''Numerical predictions for model No. 1.'' *Proc., Int. Conf. on the Verification of Numerical Procedures for the Analysis of Soil Liquefaction Problems*, K. Arulanandan and R. F. Scott, eds., Balkema, Rotterdam, The Netherlands, 1, 45–66.

Balakrishnan, A., and Kutter, B. L. (1999). ''Settlement, sliding, and liquefaction remediation of layered soil.'' *J. Geotech. Geoenviron. Eng.*, 125(11), 968–978.

Bardet, J. P., Huang, Q., and Chi, S. W. (1993). ''Numerical prediction for model No. 1.'' *Proc., Int. Conf. on the Verification of Numerical Procedures for the Analysis of Soil Liquefaction Problems*, K. Arulanandan and R. F. Scott, eds., Balkema, Rotterdam, The Netherlands, 1, 67–86.

Bazant, Z. P., and Kim, S.-S. (1979). ''Plastic-fracturing theory for concrete.'' *J. Eng. Mech. Div.*, 105(3), 407–428.

Borja, R. I., Chao, H. Y., Montans, F., and Lin, C. H. (1999). ''Nonlinear ground response at Lotung LSST site.'' *J. Geotech. Geoenviron. Eng.*, 125(3), 187–197.

Byrne, P. M., and McIntyre, J. (1994). ''Deformations in granular soils due to cyclic loading.'' *Proc., Settlement 94*, Geotechnical Special Publ. No. 40, ASCE, Reston, Va., 1864–1896.

Casagrande, A. (1936). ''Characteristics of cohesionless soils affecting the stability of earth fills.'' *J. Boston Soc. Civ. Eng.*, 23, 13–33.

Casagrande, A. (1975). ''Liquefaction and cyclic deformation of sands—A critical review.'' *Proc., 5th Pan-American Conf. on Soil Mechanics and Foundation Engineering*, also published as *Harvard soil mechanics series No. 88*, January, 1976, Harvard Univ., Cambridge, Mass.

Castro, G. (1969). ''Liquefaction of sands.'' *Harvard soil mechanics series No. 81*, Harvard Univ., Cambridge, Mass.

Chan, A. H. C. (1988). ''A unified finite element solution to static and dynamic problems in geomechanics.'' PhD dissertation, Univ. College of Swansea, Swansea, U.K.

Chen, W. F., and Mizuno, E. (1990). *Nonlinear analysis in soil mechanics, theory and implementation*, Elsevier, New York.

Cubrinovski, M., and Ishihara, K. (1998a). ''Modeling of sand behavior based on state concept.'' *Soils Found.*, 38(3), 115–127.

Cubrinovski, M., and Ishihara, K. (1998b). ''State concept and modified elastoplasticity for sand modeling.'' *Soils Found.*, 38(4), 213–225.

Dafalias, Y. F., and Manzari, M. T. (1999). ''Modeling of fabric effect on the cyclic loading response of granular soils.'' *Proc., 13th ASCE Engineering Mechanics Conf.*, ASCE, Reston, Va.

Dobry, R., and Abdoun, T. (1998). ''Posttriggering response of liquefied sand in the free field and near foundations.'' *Proc., Geotechnical Earthquake Engineering and Soil Dynamics III*, P. Dakoulas, M. Yegian, and R. D. Holtz, eds., ASCE Geotechnical Special Publ. No. 75, Vol. 2, ASCE, Reston, Va., 270–300.

Dobry, R., and Taboada, V. M. (1994). ''Possible lessons from VELACS model No. 2 results.'' *Proc., Int. Conf. on Verification of Numerical Procedures for the Analysis of Soil Liquefaction Problems*, K. Arulanandan and R. F. Scott, eds., Balkema, Rotterdam, The Netherlands, 2, 1341–1352.

Dobry, R., Taboada, V., and Liu, L. (1995). ''Centrifuge modeling of liquefaction effects during earthquakes.'' *Keynote Lecture, Proc., 1st Int. Conf. on Earthquake Geotechnical Engineering (IS-Tokyo)*, K. Ishihara, ed., Balkema, Rotterdam, The Netherlands, 3, 1291–1324.

Duncan, J. M., and Chang, C. Y. (1970). ''Nonlinear analysis of stress and strain in soils.'' *J. Soil Mech. Found. Div.*, 96(5), 1629–1653.

Hill, R. (1950). *The mathematical theory of plasticity*, Oxford University Press, London.

Iai, S. (1991). ''A strain space multiple mechanism model for cyclic

behavior of sand and its application.'' *Earthquake Engineering Research Note No. 43*, Port and Harbor Research Institute, Ministry of Transport, Japan.
Iai, S. (1998). ''Seismic analysis and performance of retaining structures.'' *Proc., Geotechnical Earthquake Engineering and Soil Dynamics III*, P. Dakoulas, M. Yegian, and R. D. Holtz, eds., Geotechnical Special Publ. No. 75, Vol. 2, ASCE, Reston, Va., 1020–1044.
Ibsen, L. B. (1994). ''The stable state in cyclic triaxial testing on sand.'' *Soil Dyn. Earthquake Eng.*, 13, 63–72.
Ishihara, K., Tatsuoka, F., and Yasuda, S. (1975). ''Undrained deformation and liquefaction of sand under cyclic stresses.'' *Soils Found.*, 15(1), 29–44.
Iwan, W. D. (1967). ''On a class of models for the yielding behavior of continuous and composite systems.'' *J. Appl. Mech.*, 34, 612–617.
Jefferies, M. G. (1993). ''Nor-sand: A simple critical state model for sand.'' *Geotechnique*, 43(1), 91–103.
Kabilamany, K., and Ishihara, K. (1990). ''Stress dilatancy and hardening laws for rigid granular model of sand.'' *Soil Dyn. Earthquake Eng.*, 9(2), 66–77.
Kondner, R. L. (1963). ''Hyperbolic stress–strain response: Cohesive soils.'' *J. Soil Mech. Found. Div.*, 89(1), 115–143.
Kramer, S. L. (1996). *Geotechnical earthquake engineering*, Prentice–Hall, Upper Saddle River, N.J.
Lacy, S. (1986). ''Numerical procedures for nonlinear transient analysis of two-phase soil system.'' PhD dissertation, Princeton Univ., Princeton, N.J.
Ladd, C. C., Foott, R., Ishihara, K., Schlosser, F., and Poulos, H. G. (1977). ''Stress-deformation and strength characteristics.'' *State-of-the-Art Report, Proc., 9th Int. Conf. on Soil Mechanics and Foundation Engineering*, Japanese Society of Soil Mechanics and Foundation Engineering, Tokyo, 2, 421–494.
Lambe, T. W., and Whitman, R. V. (1969). *Soil mechanics*, Wiley, New York.
Li, X. S., and Dafalias, Y. F. (2000). ''Dilatancy for cohesionless soils.'' *Geotechnique*, 50(4), 449–460.
Li, X. S., Ming, H. Y., and Cai, Z. Y. (2000). ''Constitutive modeling of flow liquefaction and cyclic mobility.'' *Computer simulation of earthquake effects*, K. Arulanandan, A. Anandarajah, and X. S. Li, eds., ASCE Geotechnical Special Publ. No. 110, ASCE, Reston, Va., 81–98.
Manzari, M. T., and Dafalias, Y. F. (1997). ''A critical state two-surface plasticity model for sands.'' *Geotechnique*, 49(2), 252–272.
Mroz, Z. (1967). ''On the description of anisotropic work hardening.'' *J. Mech. Phys. Solids*, 15, 163–175.
Muraleetharan, K. K., Mish, K. D., and Arulanandan, K. (1994). ''A fully coupled nonlinear dynamic analysis procedure and its verification using centrifuge test results.'' *Int. J. Numer. Analyt. Meth. Geomech.*, 18, 305–325.
National Research Council. (1985). ''Liquefaction of soils during earthquakes.'' *Report*, Committee on Earthquake Engineering, National Research Council, National Academies Press, Washington, D.C.
Nemat-Nasser, S., and Tobita, Y. (1982). ''Influence of fabric on liquefaction and densification potential of cohesionless sand.'' *Mech. Mater.*, 1, 43–62.
Papadimitriou, A. G., Bouckovalas, G. D., and Dafalias, Y. F. (2001). ''Plasticity model for sand under small and large cyclic strains.'' *J. Geotech. Geoenviron. Eng.*, 127(11), 973–983.
Parra, E. (1996). ''Numerical modeling of liquefaction and lateral ground deformation including cyclic mobility and dilation response in soil systems.'' PhD thesis, Dept. of Civil Engineering, Rensselaer Polytechnic Inst., Troy, N.Y.
Pastor, M., and Zienkiewicz, O. C. (1986). ''A generalized plasticity hierarchical model for sand under monotonic and cyclic loading.'' *Proc., 2nd Int. Symp. on Numerical Models in Geomechanics*, G. N. Pande and W. F. Van Impe, eds., Jackson and Son, Ghent, Belgium, 131–150.
Prevost, J. H. (1985). ''A simple plasticity theory for frictional cohesionless soils.'' *Soil Dyn. Earthquake Eng.*, 4(1), 9–17.
Proubet, J. (1991). ''Application of computational geomechanics to description of soil behavior.'' PhD dissertation, Univ. of Southern California, Los Angeles.
Seed, H. B. (1979). ''Soil liquefaction and cyclic mobility evaluation for level ground during earthquakes.'' *J. Geotech. Eng.*, 105(2), 201–255.
Seed, H. B., and Lee, K. L. (1966). ''Liquefaction of saturated sands during cyclic loading.'' *J. Soil Mech. Found. Div.*, 92(6), 105–134.
Sture, S., Costes, N. C., Batiste, S. N., Lankton, M. R., Al Shibli, K. A., Jeremic, B., Swanson, R. A., and Frank, M. (1998). ''Mechanics of granular materials at low effective stresses.'' *J. Aerosp. Eng.*, 11(3), 67–72.
Taboada, V. M. (1995). ''Centrifuge modeling of earthquake-induced lateral spreading in sand using a laminar box.'' PhD thesis, Rensselaer Polytechnic Institute, Troy, N.Y.
Tateishi, A., Taguchi, Y., Oka, F., and Yashima, A. (1995). ''A cyclic elasto-plastic model for sand and its application under various stress conditions.'' *Proc., 1st Int. Conf. on Earthquake Geotechnical Engineering*, Balkema, Rotterdam, The Netherlands, 1, 399–404.
Wang, Z. L., Dafalias, Y. F., and Shen, C. K. (1990). ''Bounding surface hypoplasticity model for sand.'' *J. Eng. Mech.*, 116(5), 983–1001.
Yang, Z. (2000). ''Numerical modeling of earthquake site response including dilation and liquefaction.'' PhD dissertation, Dept. of Civil Engineering and Engineering Mechanics, Columbia University, New York.